Appendix 4

Section 4 *Posterior Time-Step Adjustment Technique in Substructuring Pseudo-Dynamic Test*

presented by K. Kusunoki

Fifth International Congress on Advances in Civil Engineering, 25-27 September 2002
Istanbul Technical University, Istanbul, Turkey

POSTERIOR TIME-STEP ADJUSTMENT TECHNIQUE IN SUBSTRUCTURING PSEUDO-DYNAMIC TEST
- Numerical simulation and loading test-

K. KUSUNOKI
Building Research Institute, Department of Structural Engineering, Tsukuba, Japan

Waon-Ho Yi
Kwang Woon University, Department of Architectural Engineering, Seoul, Korea

Abstract

The pseudo-dynamic test is a hybrid testing method consisting of a numerical simulation of the earthquake response by using a numerical model and a loading test of a specimen. The pseudo-dynamic testing technique has been applied to various seismic experiments since it has advantages over the shaking table test, i.e. enables us to study dynamic behaviors of relatively large-scale structures. However, experimental errors are inevitable in the pseudo-dynamic test. Some of these errors cannot be eliminated due to limitations in control system. It is often reported that dynamic responses of testing structures are much affected by cumulative control errors. To minimize the control errors in the pseudo-dynamic test, two numerical integration techniques, PTA (Posterior Timestep Adjustment technique) and MPTA (Modified PTA) are proposed herein. A posterior adjustment of the time increment from a fixed value of Δt to an adjusted value was performed to minimize the effect of the control errors in PTA and MPTA techniques. In this paper, the testing procedures and the proposed numerical technique are reviewed. First, a numerical simulation of a linear and non-linear response analyses with Multi-Degree-of-Freedom (MDF) model by considering an undershooting control error at the first story (the first story was supposed as a testing story) was carried out. Then a pseudo-dynamic loading tests with a second-degree-of-freedom system of which the first story was experimentally loaded were conducted. In the above two series, both the PTA and the MPTA were performed, and their validity to minimize the control error is discussed

Introduction

The substructuring pseudo-dynamic test (referred to as SPT test subsequently) is a hybrid method. The restoring force vectors calculated in a computer with numerical hysteresis models and measured from a loading test are combined into a global restoring

force vector for the whole structure at each numerical integration step. It has advantages over the shaking table test by studying the dynamic response of relatively large-scale structures.

Computer-controlled actuators are usually applied to the loading system of SPT tests. It is well accepted that random error appears at measuring and controlling instruments. Furthermore, control error can also occur in an actuator control system. These errors are significantly affecting the accuracy of SPT test [Kabayama, 1995]. New integration techniques in which time-step is adjusted to reduce the effects of the control error, PTA and MPTA are proposed herein. The purpose of this paper is to estimate the stability and the accuracy of these techniques for an SPT test.

Control error

Actuators are usually controlled with analogue voltage. On the other hand, computers are digitally controlled. Signals of the loading system therefore must be controlled through the Analogue-Digital and Digital-Analogue transfer (referred to as A/D and D/A transfer subsequently). A minimum controllable displacement $\delta_{\min}$ depends on the precision of the A/D and D/A transfer, and it can be given as follows.

$$\delta_{\min} = \frac{2\ell}{2^n} \tag{1}$$

In this Equation, $\pm\ell$ represents an actuator stroke length and 2^n represents the precision of the A/D and D/A transfer board in a computer. It is impossible to control an actuator closer to a target displacement if the distance from a target displacement is less than $\delta_{\min}$ (Fig. 1(a)). Usually the undershooting error is applied to define the target displacement in order to avoid the damage to a specimen caused by the overshooting displacement. If the undershooting error is applied, the measured displacement does not reach the exact target displacement at each step. Thus, the hysteresis characteristic used in a numerical integration becomes different from that of a real specimen. Especially when the response displacement is relatively small in linear domain. For the latter, the hysteresis curve shows an anti-clockwise loop (Fig. 1 (b)). Although the value of the control error is very small, the calculated response is much amplified compared with the real response leading to an additional energy input caused by the anti-clockwise loop [Kabayama, 1995].

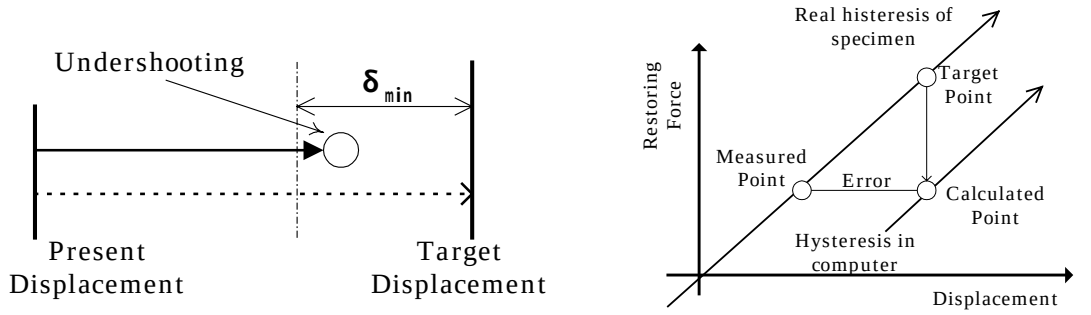

(a) Undershooting control error

(b) The effect of undershooting control error

Fig. 1: Undershooting control error and its effects

Posterior time-step adjustment technique (PTA)

It can be said that an appropriate response cannot be calculated with the SPT test using the Operator-Splitting (OS) integration technique [Nakashima et. al., 1990], which does not consider the effect of the control error. In this section, procedures of the PTA technique based on the OS technique, which reduces the effect of control error, are introduced [Yi and Peek, 1993]. The value of the control error displacement measured in an SPT test is calculated from the difference between the predictor displacement $\{y^*_{n+1}\}$ (Eq. (2)) and the measured displacement $\{\tilde{y}^*_{n+1}\}$ of the experimental portion in the SPT test. The new predictor displacement vector $\{\tilde{y}^{**}_{n+1}\}$ with variable time-step Δt_n is then defined by Eq. (3);

$$\{y^*_{n+1}\} = \{y_n\} + \{\dot{y}_n\}\Delta t + \frac{1}{4}\{\ddot{y}_n\}\Delta t^2 \tag{2}$$

$$\{\tilde{y}^{**}_{n+1}\} = \{y_n\} + \{\dot{y}_n\}\Delta t_n + \frac{1}{4}\{\ddot{y}_n\}\Delta t_n{}^2 \tag{3}$$

And the value of the variable time-step Δt_n, which minimizes the norm $\| \{\tilde{y}^*_{n+1}\} - \{\tilde{y}^{**}_{n+1}\} \|$, can be found through the Newton-Raphson convergent technique. The effect of the control error on the response displacement at n-th step obtained from Eq. (4) can be reduced using Δt_n instead of Δt and $\{\tilde{y}^{**}_{n+1}\}$ instead of $\{y^*_{n+1}\}$. In other words, Δt_n is the appropriate time-step, which minimizes the difference between the predictor and the measured displacement of a specimen.

$$[M]\{\ddot{y}_{n+1}\} + [C]\{\dot{y}_{n+1}\} + \{Q^*_{n+1}\} + [K^I]\left(\{y_{n+1}\} - \{y^*_{n+1}\}\right) = -[M]\{\ddot{y}^0_{n+1}\} \tag{4}$$

In order to reduce the control error of both experimental and numerical portion, the whole displacement data is used to calculate the norm (Fig. 2 (a)). The norm of the whole displacement vector is generally formulated as Eq. (5). If the weight matrix [G] can be determined properly, an appropriate Δt_n can be obtained. However, it can be accepted that it is difficult to define [G] properly. A time range parameter θ needs to be determined in order to avoid a negative or relatively large Δt_n value as shown in Eq. (6).

$$\| \{\tilde{y}^*_{n+1}\} - \{\tilde{y}^{**}_{n+1}\} \| = \sqrt{\left(\{\tilde{y}^*_{n+1}\} - \{\tilde{y}^{**}_{n+1}\}\right)^t [G] \left(\{\tilde{y}^*_{n+1}\} - \{\tilde{y}^{**}_{n+1}\}\right)} \tag{5}$$

$$\left(\Delta t_{n\min}, \Delta t_{n\max}\right) = \left[(1-\theta)\Delta t, (1+\theta)\Delta t\right] \tag{6}$$

Modified posterior time-step adjustment technique (MPTA)

As mentioned in the previous section, it is difficult to determine the appropriate weight matrix [G] in the PTA technique. As a result, an appropriate Δt_n can not be found by the PTA technique. To overcome this disadvantage of this technique, a new method, MPTA is considered. In the latter, the whole structure is divided into a numerical and experimental portions. The value of Δt_n is calculated from only the displacement data of the experiment portion, which contains the control error. In this section, the procedures

of the MPTA technique are introduced. In these procedures, force and displacement vectors of the whole structure $\{\ \}$ need to be divided into an experimental portion $\{\ \}_E$ and a numerical portion $\{\ \}_A$ through re-assembling nodal numbers appropriately so that $\{\ \}^t$ can form $\left\{\{\ \}_E^t, \{\ \}_A^t\right\}$.

Firstly, the predictor displacement value of the testing portion $\left\{ y_{n+1}^* \right\}_E$ is calculated with a fixed time-step Δt. Then $\left\{ y_{n+1}^* \right\}_E$ is imposed to the actuator as a target displacement. The restoring force vector $\left\{ Q_{n+1}^* \right\}_E$ and the displacement vector $\left\{ \tilde{y}_{n+1}^* \right\}_E$ of the experimental portion are measured when the distance between the target displacement and the measured displacement of a specimen is less than $\delta_{\min}$ (Fig. 2 (c)). The variable time-step Δt_n, which minimizes the norm $\left\| \left\{ \tilde{y}_{n+1}^* \right\}_E - \left\{ \tilde{y}_{n+1}^{**} \right\}_E \right\|$, can be found with the Newton-Raphson convergent technique. The equation of this norm is defined by Eqs. (7) and (8), where [I] represents the unit matrix.

$$\left\{ \tilde{y}_{n+1}^{**} \right\}_E = \{ y_n \}_E + \{ \dot{y}_n \}_E \Delta t_n + \frac{1}{4} \{ \ddot{y}_n \}_E \Delta t_n^{\,2} \tag{7}$$

$$\left\| \left\{ \tilde{y}_{n+1}^{*} \right\}_E - \left\{ \tilde{y}_{n+1}^{**} \right\}_E \right\| = \sqrt{\left(\left\{ \tilde{y}_{n+1}^{*} \right\}_E - \left\{ \tilde{y}_{n+1}^{**} \right\}_E \right)^t [I] \left(\left\{ \tilde{y}_{n+1}^{*} \right\}_E - \left\{ \tilde{y}_{n+1}^{**} \right\}_E \right)} \tag{8}$$

The predictor displacement vector of the numerical portion $\left\{ y_{n+1}^* \right\}_A$ can be calculated with Δt_n as Eq. (9) (Fig. 2 (c)). The restoring force vector of the numerical portion $\left\{ Q_{n+1}^* \right\}_A$ at $\left\{ y_{n+1}^* \right\}_A$ can be calculated with the numerical model.

$$\left\{ y_{n+1}^* \right\}_A = \{ y_n \}_A + \{ \dot{y}_n \}_A \Delta t_n + \frac{1}{4} \{ \ddot{y}_n \}_A \Delta t_n^{\,2} \tag{9}$$

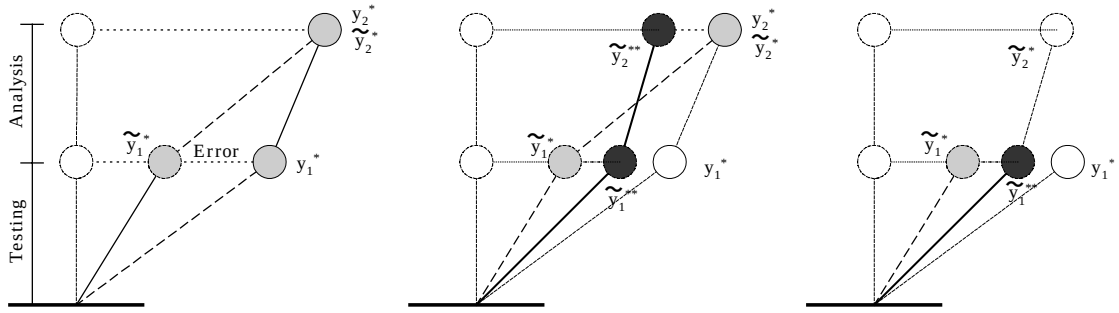

(a) SPT test (b) PTA Technique (C) MPTA Technique

Fig. 2: SPT test with the PTA and the MPTA techniques for a two-degree-of-freedom system

The restoring force vector of the whole structure $\left\{ Q_{n+1}^* \right\}$ can be calculated by combining $\left\{ Q_{n+1}^* \right\}_E$ and $\left\{ Q_{n+1}^* \right\}_A$. Finally the response displacement vector at (n+1)-th step $\{ y_{n+1} \}$ can be obtained from Eq. (4) and Δt_n. The range of Δt_n is defined by Eq. (6) in order to avoid a negative or relatively large Δt_n value as mentioned earlier.

If the increment of the predictor displacement of the experimental portion at n-th step $\left\{ \Delta y_n^* \right\}_E$ is less than $\delta_{\min}$, the actuator maintains the present position (Fig. 3 (a)). If the

increment of the measured displacement is zero, Δt_n always becomes negative or zero. Then Δt is used in Eq. (4) instead of Δt_n, and the restoring force of the experimental portion is calculated numerically with a linear extrapolation technique (Fig. 3 (b)).

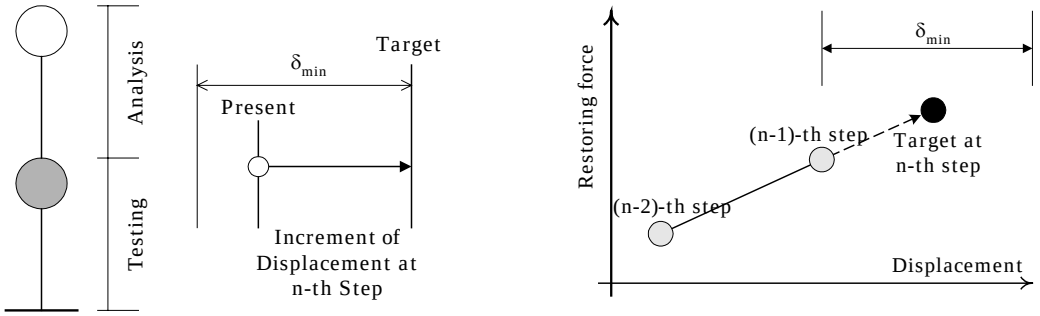

(a) Increment displacement becomes zero (b) Linear extrapolation method

Fig. 3: Linear extrapolation method

Numerical examination with PTA and MPTA

Linear and non-linear dynamic response analyses were carried out with a six-degree-of-freedom shear mode vibration system (referred to as MDF subsequently) by considering the effect of the control error numerically to estimate the basic characteristics of the PTA and the MPTA. The first story was assumed as an experimental portion. The unit matrix [I] was used as the weight matrix of the PTA in this paper.

The weight of each floor was 172.80 tonf and the height of each story was 4.0m. The damping coefficient was assumed 0.0%, since the main purpose of this paper is to investigate the effect of the control error. Takeda Tri-Linear Model was used as a hysteresis model of each story [Takeda et. al., 1970]. The restoring forces and the displacements at each stiffness degradation point were calculated and each parameter of the MDF is listed in Table. 1.

Table. 1: Parameters list for SDF and MDF (tonf, cm) [AIJ, 1992]

System	Story	Fc	Dc	Fy	Dy	Fu	Du
MDF	1	108.00	0.36	324.00	2.67	327.24	13.33
	2	98.74	0.36	296.23	2.67	325.85	13.33
	3	88.87	0.36	266.61	2.67	293.27	13.33
	4	80.23	0.36	240.69	2.67	264.75	13.33
	5	63.36	0.36	190.08	2.67	209.09	13.33
	6	37.03	0.36	111.09	2.67	122.19	13.33

1. Fy ; Ultimate lateral resistance in each story (base shear coefficient is assumed 0.3).
2. Dy = Story height/150.
3. Fc = Fy / 3.0.
4. Dc ; Calculated with Fc, elastic stiffness and stiffness degrading ratio (0.4).
5. Fu, Du ; Calculated so that post yielding stiffness $Fu - Fy/Du - Dy$ is Fc/Dc times 1/1000.

The input acceleration records for the pseudo-dynamic test conducted by Kabayama et al. was used as the input earthquake data by scaling its peak acceleration to 500 gal (Fig.

4).

The Max/Min stroke length of the actuator was assumed $\pm 15cm$ and the precision of the A/D and D/A transfer board were adjusted 11 bits. As a result, $\delta_{\min}$ was 0.0146 cm. The undershooting control error was applied and the value of the undershooting control error was calculated to simulate the SPT test with $\delta_{\min}$ in each step. The parameter θ and the weight matrix were assumed 0.5 and unit matrix [I], respectively. It should be noted that the PTA and the MPTA techniques proposed in this paper can be applied to both the undershooting and the overshooting control errors.

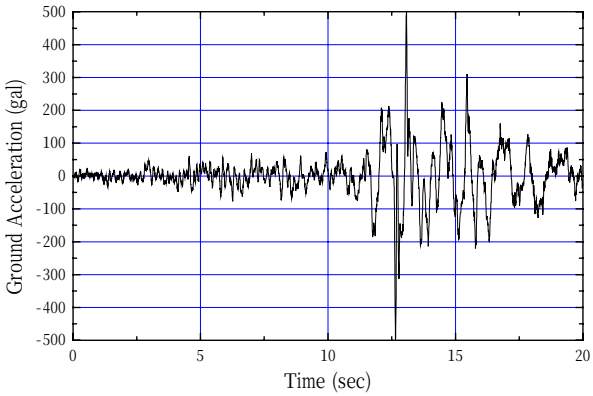

Fig. 4: The input earthquake data

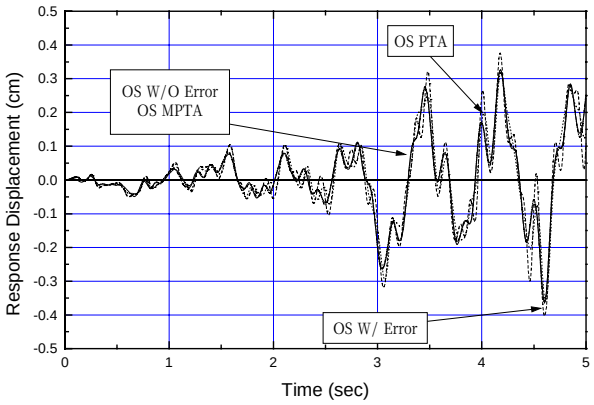

(a) Response displacements at the first story (Linear:6DF:0~10 sec)

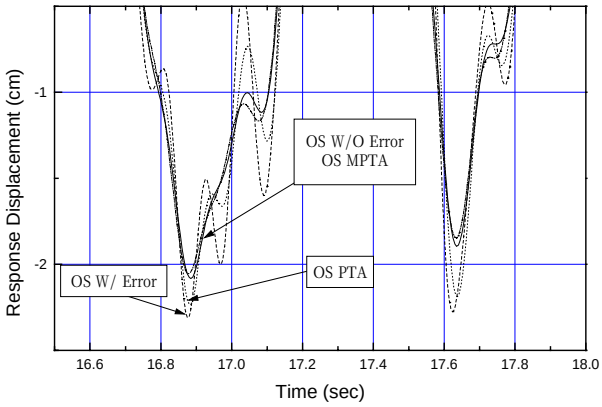

(b) Response displacements at the first story (Linear:6DF:16.5~18 sec)

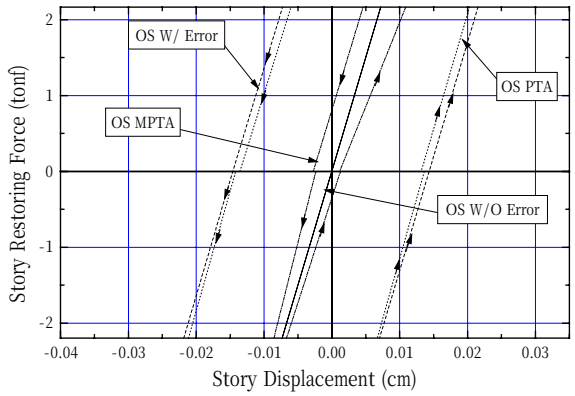

(c) Enveloped curves of the story restoring force- story displacement relationship (Linear:6DF)

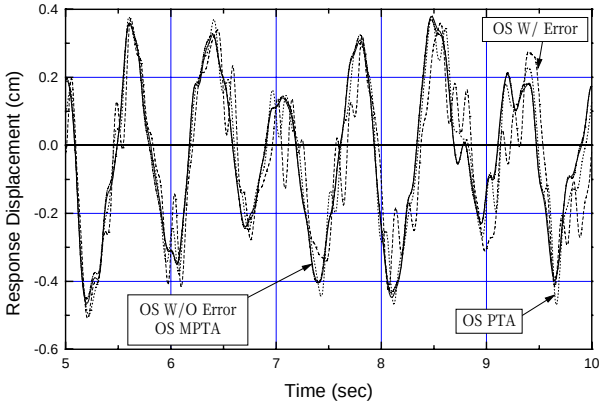

(d) Response displacements (Non-linear:6DF:5~10 sec)

(W/: with, W/O: without)

Fig. 5: Linear and non-linear responses of MDF system

MDF SYSTEM

Fig. 5 (a) and (b) show the time histories of linear response displacement at the first story. It can be said that the response displacement of the OS /W Error was amplified compared with that of the OS W/O Error. The spurious high mode effect of the OS W/ Error was predominant because of the undershooting control error [Nakashima et. al., 1982 and 1983]. Furthermore, the PTA could not reduce the effect of the control error, and the spurious high mode effect of the PTA was also predominant as a result of the OS W/ Error. One of the reasons that the PTA cannot reduce the effect of the undershooting control error is the assumption of [G]=[I]. One can easily imagine that it is difficult to define the weight matrix [G] properly. On the other hand, the MPTA reduced the effect of the undershooting control error sufficiently. Thus the response of the MPTA was almost the same as the OS W/O Error. As shown in Fig. 5 (c), structural responses calculated using OS W/ Error, PTA and MPTA techniques showed anti-clockwise hysteresis loops. However, the area of the MPTA was smaller than that of the OS W/ Error and the PTA. Hence its response was successfully improved.

Fig. 5 (d) shows the time histories of a non-linear response displacement. The responses of the OS W/ Error and the PTA were amplified by the effect of the undershooting control error. Therefore, the spurious high mode effect of these responses was predominant as was found in the linear analysis results. As a result, the MPTA reduced the effect of control error sufficiently and the response of the MPTA agreed very well with the OS W/O Error.

Pseudo-dynamic test with Second-degree-of-freedom system

In order to confirm the validity of the MPTA technique, substructuring pseudo-dynamic test with a second-degree-of-freedom system were conducted. The structure was modeled so as to represent a shear vibration mode system. The first story was the test story that was experimentally loaded, and the responses of the second story were calculated within a computer. Since the purpose of this test was not to simulate the actual response of the structure but to confirm the validity of the MPTA technique, the hysteretic characteristics of each story were assumed as listed in Table 1, and the damping coefficient was assumed as 0.0%. The fixed time-step Δt of 0.01 sec was applied.

Outline of specimen and loading system

The dimension of the specimen is shown in Fig. 6. The hysteretic characteristics of the

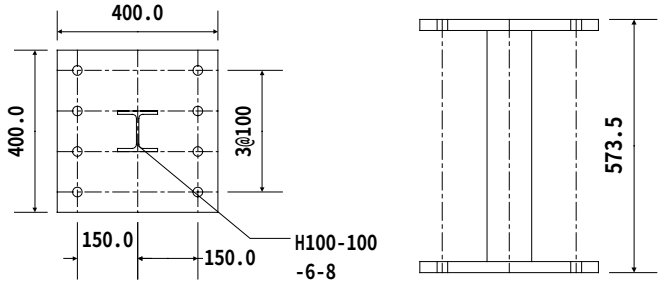

Fig. 6: Dimension of the specimen

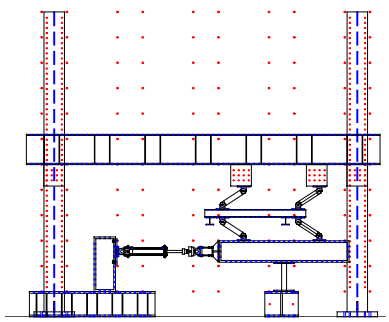

Fig. 7: The Loading system

specimen are listed on Table 1. The H-shaped steel of 100*100*6*8 was used to represent the response characteristics of the first story.

The loading system is shown in Fig.7. One actuator was used to apply a lateral force to the specimen. A pantograph system was attached on the loading beam to hold the reflection point of the specimen at mid-height of the specimen. The total weight of the loading beam, actuator, and pantograph was canceled by the counter weight.

Table 1: Hysteretic characteristics of the specimen

Direction	My (N·cm)	Qy (N)	Ke(N/cm)	Dy (cm)
X	2.893×10^{6}	3.998×10^{4}	6.352×10^{5}	1.740×10^{-1}
Y	1.929×10^{6}	1.105×10^{4}	2.2985×10^{5}	1.740×10^{-1}

Input earthquake data

The NS component of 1987 Chiba-Ken-Toho-Oki earthquake data recorded at Chiba Experimental Station of Institute of Industrial Science, University of Tokyo, was used as the input earthquake data. Twenty seconds record including the peak ground acceleration was used. Fig. 8 shows the input earthquake data.

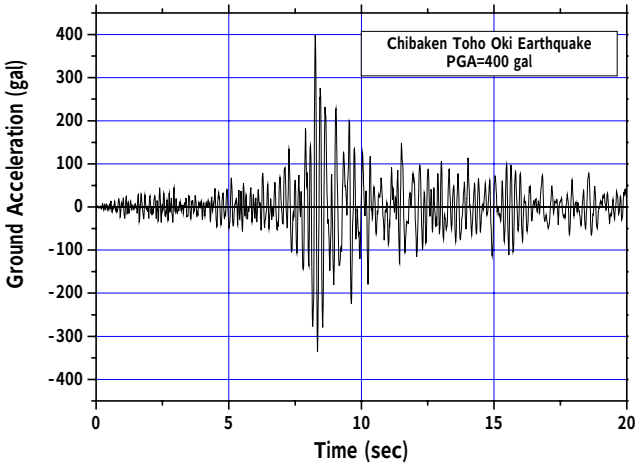

Fig. 8: Input earthquake data (Chibaken-Toho-Oki earthquake)

Test parameter

The test parameter was the actuator control precision, the precisions of the D/A transfer were 8-bit and 12-bit. It was found from the preliminary test results that the precision of 12-bit was the upper bound to control the actuator. The tests with and without the MPTA technique at the precision of 8-bit were conducted. Furthermore, a precision of 12-bit was applied to the test of which the first and second floors were loaded. The different test cases are listed on Table 2. The minimum controllable displacements for

Table 2: Details of the test case

Test case	First story	Second story	MPTA Technique
Case 1	Loaded (8Bit)	Numerical Simulation	Not used
Case 2	Loaded (8Bit)	Numerical Simulation	Used
Case 3	Loaded (12Bit)	Numerical Simulation	Not used
Case 4	Loaded (12Bit)	Loaded (12Bit)	Not used

each precision of the D/A board can be calculated as follows;

for 8-bit; $\frac{5\times 2}{2^8} = 0.0390625\,(\text{cm})$, and for 12-bit; $\frac{5\times 2}{2^{12}} = 0.0024414(\text{cm})$

Test results

The test durations are listed on Table 3. Since the undershooting error was applied to control the actuator, the test with the MPTA technique (case 2) needed 759 steps more than the test with fixed time-step. The test durations of case 1 and case 2, of which the D/A precision were 8-bit, were approximately 3 and 4 hours, respectively. They are allowably short to conduct the substructuring pseudo-dynamic test. It can be said that the MPTA technique does not extend the test duration too much. On the other hand, the test durations of case 3 and case 4, of which D/A precision were 12-bit, were approximately 12 and 22 hours, respectively. They were almost 4 to 8 times as long as case 1 and case 2.

Table 3: Test durations

Case	Steps	Duration	Date
Case 1	2000	3:18	9/18
Case 2	2759	4:11	9/18
Case 3	2000	11:01	9/14～15
Case 4	2000	22:02	9/4～5

The time history of the response displacement on the second floor is shown in Fig. 9. It can be seen, especially, among the middle response region that the response displacement of case 1 was amplified due to the control error. On the contrary, the responses with the precision of 12bit (case 3) were slightly reduced compared with the numerical analysis result. Moreover, the responses with the precision of 12bit were observed to shift in the large response region. The response with the MPTA technique (case 2), however, agreed very well with the numerical analysis result.

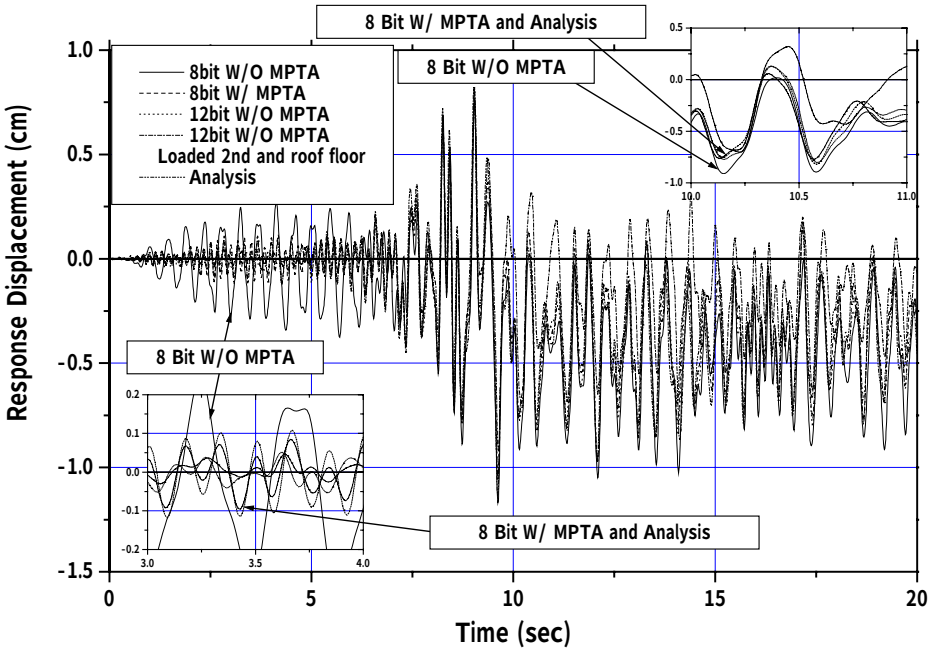

Fig. 9: Time history of the response displacement at the second floor

Concluding remarks

The Posterior Time-step Adjustment technique and the Modified PTA technique were proposed in order to reduce the effect of the control error. Linear and non-linear dynamic response analyses of the MDF shear vibration mode system considering the undershooting actuator control error at the first story was carried out. In addition, the substructuring pseudo-dynamic tests with a second-degree-of-freedom system were conducted. Results obtained from the investigation can be summarized as follows;

1) Dynamic responses are amplified by the effect of undershooting control error, and the spurious high mode effect of the MDF responses is predominant.
2) The Modified PTA technique can reduce the effect of the control error successfully for both linear and non-linear responses of the MDF systems, while the PTA technique cannot reduce it if the weight matrix of the PTA is not provided properly.
3) The modified PTA technique is a useful technique to achieve the higher accuracy of the substructuring pseudo-dynamic test with relatively low actuator control precision.
4) The modified PTA technique does not extend the test duration too much.

References

AIJ/Architectural Institute of Japan (1992), “Design Guidelines for Earthquake Resistant Reinforced Concrete Buildings Based on Ultimate Strength Concept”

KABAYAMA, K. (1995), “Study on High Accurate On-line Test”, Doctoral Thesis of Univ. of Tokyo

NAKASHIMA, M., KATO, H. and KAMINOSONO, T. (1982 and 1983), “Simulation of Earthquake Response by Pseudo-dynamic Test Technique Part 1, 2,3 and 4”, Summaries of technical papers of annual meeting, AIJ, pp.951-954(1982), pp.445-448 (1983), Oct.

NAKASHIMA, M., ISHIDA, M. and ANDO, K. (1990), ”Integration Techniques for Substructure Pseudo-dynamic Test (Pseudo-dynamic test using substructuring techniques)”, Journal of Struct. Constr. Engng, AIJ, No417, Nov.

Plesha, M. E. and Belytschko (1985), T., ”A Constitutive Operator Splitting Method for Nonlinear Transient Analysis”, Computers & Structures, Vol.20, No.4

Takeda, T., Mete A. Sozen, N. Norby Nielsen (1970), ”Reinforced Concrete Response to Simulated Earthquake”, Journal of Structural Division, Vol. 96, ST 12

Yi, W. H. and Peek, R. (1993), ”Posterior Time-Step Adjustment in Pseudo-dynamic Testing”, Journal of Engineering Mechanics, Vol.119, No. 7, July

KUSUNOKI, K., Nakano, Y., Yi, W. H., Lee, L. H. (2000), “Posterior Time-Step Adjustment Technique in Substructuring Pseudo-dynamic Test”, 12th world conference on earthquake engineering, Feb.

Appendix 5

Section 5 *Mass-eccentric Effect on response of Base Isolation System for Houses*

presented by M. Iiba

Mass-eccentric Effect on Response of Base Isolation System for Houses

Iiba Masanori[1], Myslimaj Bujar[2], Midorikawa Mitsumasa[1]
and Ishizaki Yohji[3]

[1]*Building Research Institute, Tsukuba, Japan*
[2]*McMaster University, Hamilton, Ontario, Canada*
[3]*Nitta Corporation, Nara, Japan*

ABSTRACT

In this paper, the effect of mass eccentricity on the response of recently developed base isolation systems for houses is discussed. Shaking table tests on base isolated models were carried out. Three patterns of weight distribution into the system were used to create three different scenarios: no mass-eccentricity, moderate mass-eccentricity and excessive mass-eccentricity. The torsional responses of two representative types for rolling and sliding systems are compared. A remarkable difference between peak torsional angle responses of the two systems was observed, with the rolling system showing a clear tendency to respond with larger torsional angle amplitudes as compared to the sliding system.

1. INTRODUCTION

Many structures were severely damaged during the 1995 Hyogoken-Nanbu Earthquake. Some of the buildings collapsed either at the 1st story or at their intermediate stories. There were also many people that were found dead or injured inside their houses. The seismic response records obtained at several base isolated structures during the 1994 Northridge earthquake and 1995 Hyogoken-Nanbu earthquake demonstrated clearly the efficiency of base isolation in increasing the building safety and in the same time contributed to the sudden increase in the demand for seismically isolated buildings right after these earthquakes.

There are some signs of a start-up for the expansion of base-isolated structures into private housing sector, but still far from what has been reported from the multi-unit housing sector. This is related to the following factors that need to be considered:

a) Cost performance
b) Relatively small weight of residential houses
c) Habitability and safety during strong winds or typhoons

In order to achieve the required performance for the isolators and base-isolated residences, the development of new types of isolators, which can be grouped in three systems: (a) Rubber bearing system, (b) Rolling system and (c) Sliding system, were focused. The main objective of

this study is the investigation of the effect of mass eccentricity on the response of the base isolation systems. Special attention is paid to the torsional response of two representative isolators belonging to the group (b) and (c).

2. EXPERIMENTAL MODELS

The experimental setup is shown in Fig. 1. It was used for testing the base-isolation system under one- and three-directional earthquake excitations, providing thus the experimental database necessary for the investigation of the effect of mass eccentricity on the response of the system. Three patterns of weight distribution into the system were used to create three mass-eccentricity scenarios: (1) no mass-eccentricity (ECC0); (2) moderate mass-eccentricity (ECC1) and (3) excessive mass-eccentricity (ECC2). Table 1 shows the location of center of gravity (CG) for each mass-eccentricity scenario in reference to the heavy side edge. Schematic drawings and fundamental characteristics of two representatives are shown in Fig. 2. The rolling system is a combination of ball bearings in the center with high damping laminated rubber in the perimeter. As for the sliding system, it is principally designed to absorb the energy through the friction between two spherical surfaces and a sliding cylinder, which are coated with a low-friction composite material. Tests were performed on a large-scale three-dimensional shaking table installed at Public Works Research Institute, Japan.

Table 1. CG location for each mass-eccentricity scenario

Mass-Eccentricity Scenario	CG location in reference to the heavy side edge (m)	CG - heavy side edge distance normalized by the isolators' spacing
ECC0	2.82	1.000
ECC1	2.55	0.905
ECC2	2.29	0.812

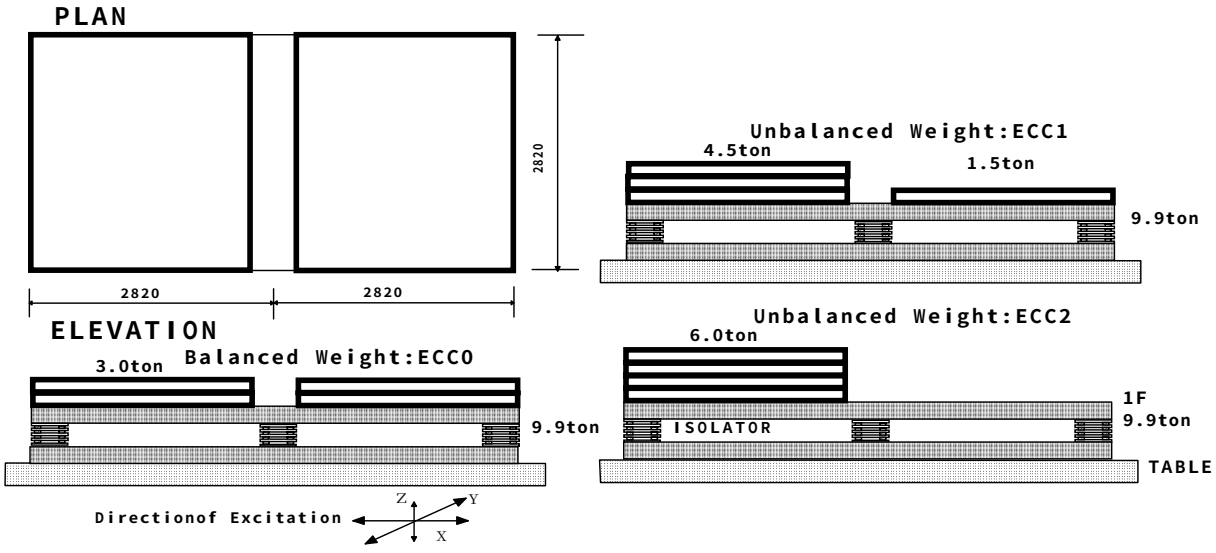

Figure 1. Base isolated model with mass eccentricity

Table 2. Adjusted PGV values for each component of the input motion

EQ Name	1940 El Centro			1995 JMA Kobe		
Direction	X	Y	Z	X	Y	Z
Actual PGV	24.8	20.4	6.32	23.1	23.9	12.4
(cm/s)	49.1	39.7	12.2	44.6	48.3	23.1

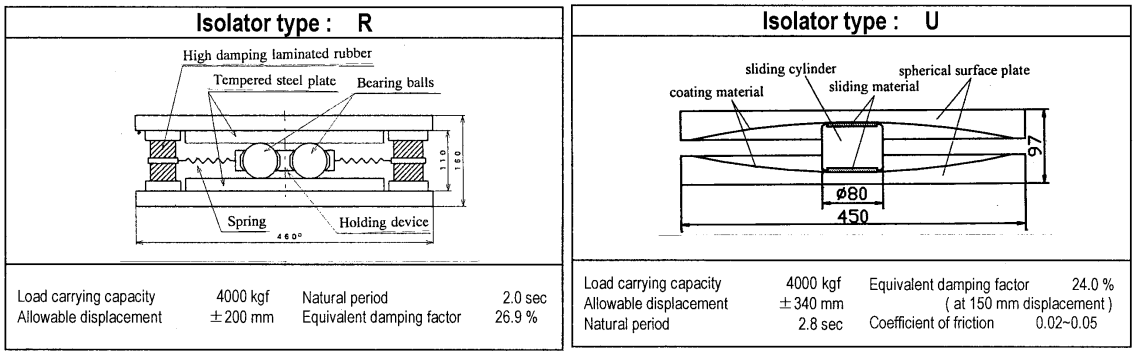

a) Rolling system **b)** Sliding system

Figure 2. An outline of fundamental characteristics of two representative isolators

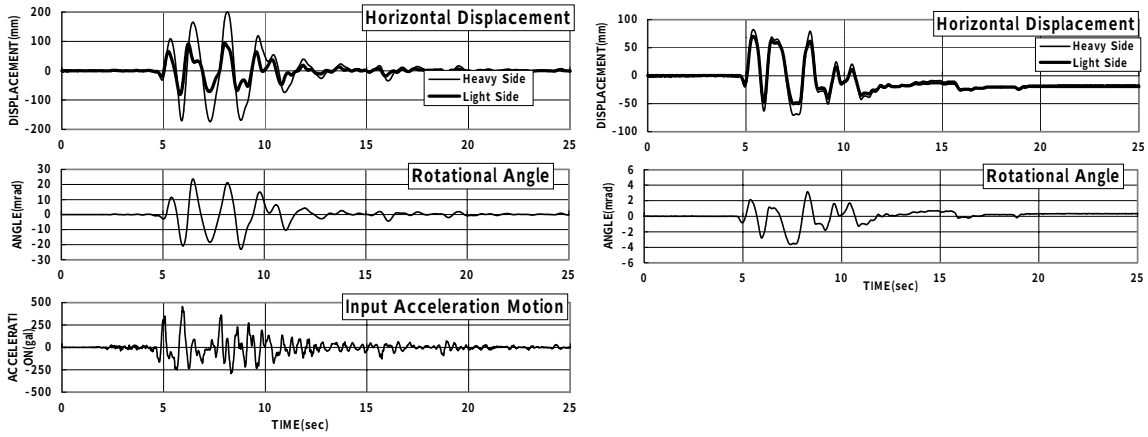

a) Rolling system b)Sliding system

Figure 3. Response time histories of rolling and sliding systems for ECC2 mass-eccentricity case

Strong ground motions recorded during the El Centro Earthquake of 1940 and Kobe Earthquake of January 17, 1995 (JMA Kobe Station record) were used as input motions at the shaking table. Based on the peak ground velocity (PGV) value observed in each record, the input earthquake waves were proportionally adjusted to the intensity levels of 25 and 50cm/s. The actual PGV values for each component of input motion are shown in Table 2.

3. SHAKING TABLE TEST RESULTS

In Fig. 3 are shown response time histories for rolling and sliding systems. They correspond to the ECC2 mass-eccentricity scenario, using only the NS component of 1995 JMA Kobe earthquake motion as seismic excitation in the Y direction. For both systems, it can be noticed that the displacement response of the heavy side is larger than that of the light side. The variation of peak displacement response at both edges with respect to mass-eccentricity ratio is shown in Fig. 4. As the mass-eccentricity increases the peak displacement response of the heavy side increases, while that one of the light side decreases. In addition, it can be noticed that the torsional effect on the displacement response of the rolling system is larger than that of the sliding system.

As shown in Fig. 5, it can be also noticed that the rolling system tends to rotate easily due to the mass-eccentricity. Figure 6 shows the relationship between shear force and horizontal displacement for the ECC0 case, using the NS component of 1995 JMA Kobe earthquake motion as seismic excitation in the Y direction. As it can be noticed from these two plots, the rolling type system delivers less hysteretic damping compared to the sliding system that shows a larger capacity in energy absorption for quite a wide range of displacement response.

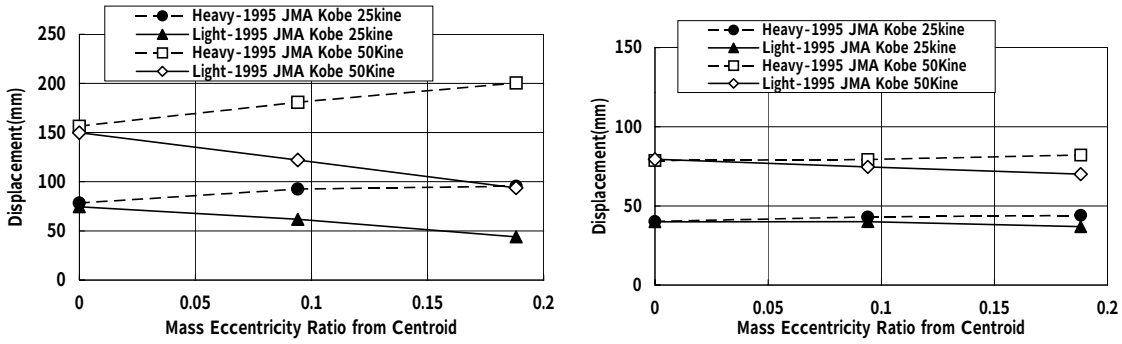

a) Rolling system b)Sliding system

Figure 4. Variation of peak edge displacement responses with mass-eccentricity ratio.

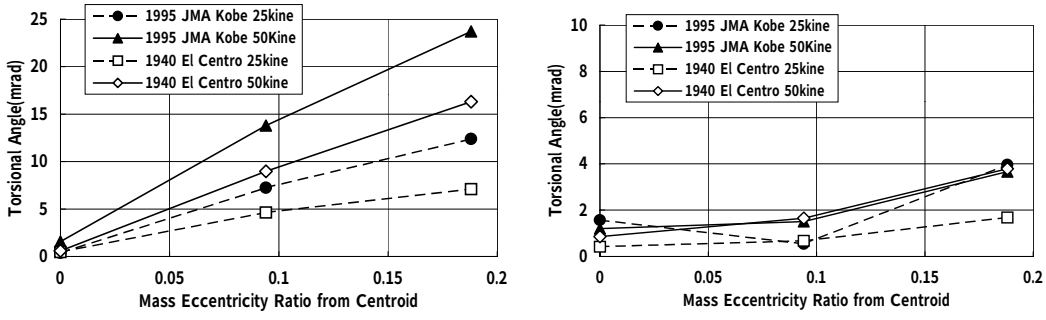

a) Rolling system b)Sliding system

Figure 5. Variation of peak torsional angle response with mass-eccentricity ratio

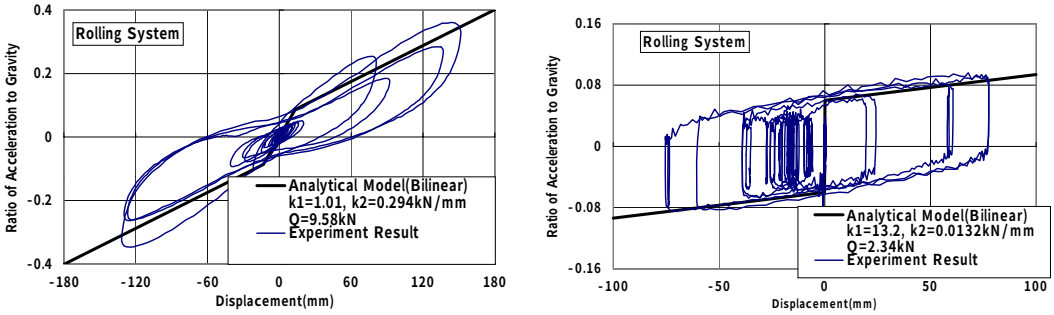

a) Rolling system b)Sliding system

Figure 6. Shear force – displacement relationship from analytical modeling and experimental data

4. ESTIMATION OF TORSIONAL RESPONSE BY STATIC PROCEDURE

An attempt is made in this section to estimate the torsional response by making use of static equilibrium. The analytical model conceived for this purpose is illustrated in Fig. 7. The displacement due to torsion is determined as follows:

a) Center of gravity: $x_g = \sum(W_i x_i) / \sum W_i$, $y_g = 0$

b) Isolator's stiffness: $K_i = K(u_{yi})$ (secant modulus, displacement dependency in Fig. 6)

c) Center of stiffness: $x_k = \sum(K_i x_i) / \sum K_i$

d) Stiffness eccentricity: $e_y = x_k - x_g$

e) Torsional angle: $\theta = \mathrm{M}_\kappa / K_t$, where $M_k = \{\sum(K_i u_{yi})\} \cdot e_y$, $K_t = \sum K_i \{(x_i - x_k)^2 + y_i{}^2\}$

f) Displacement: $u_{yi} = u_{yk} + \theta(x_k - x_i)$, where u_{yk} is displacement at the center of stiffness

The maximum response for the ECC0 mass-eccentricity case, u_{y0} , is used as an initial value for the horizontal displacement response. Since nonlinear characteristics of the isolators are taken into account, steps b) to f) are cyclically repeated until the displacement convergence is reached.

In Fig. 8 is shown the relationship between peak torsional angle response and the mass-eccentricity for the case when the NS component of JMA Kobe earthquake motion is used as seismic excitation in the Y direction. For comparison, two solid lines are also drawn in the graph representing the results obtained by the static procedure. In case of the sliding system, a good agreement is observed. It doesn't appear to be the same for the rolling system.

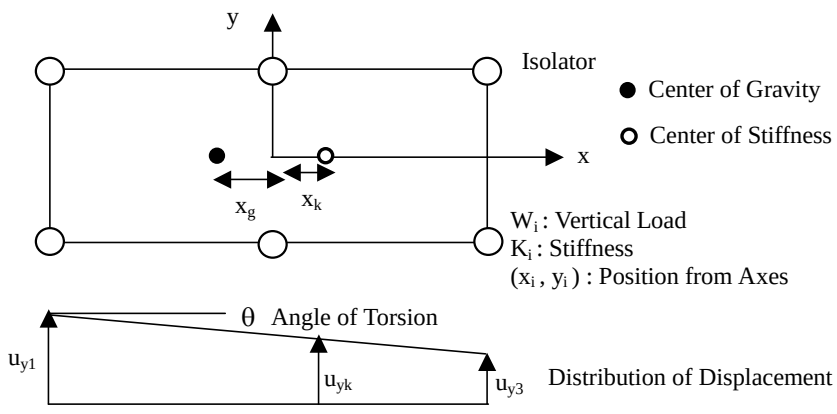

Figure 7. Simplified model used for the estimation of torsional angle response

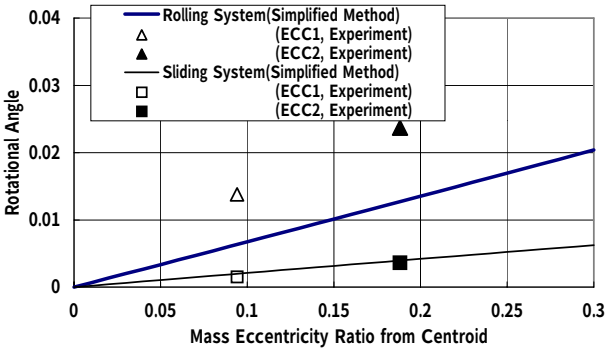

Figure 8. Comparison of peak torsional angle responses

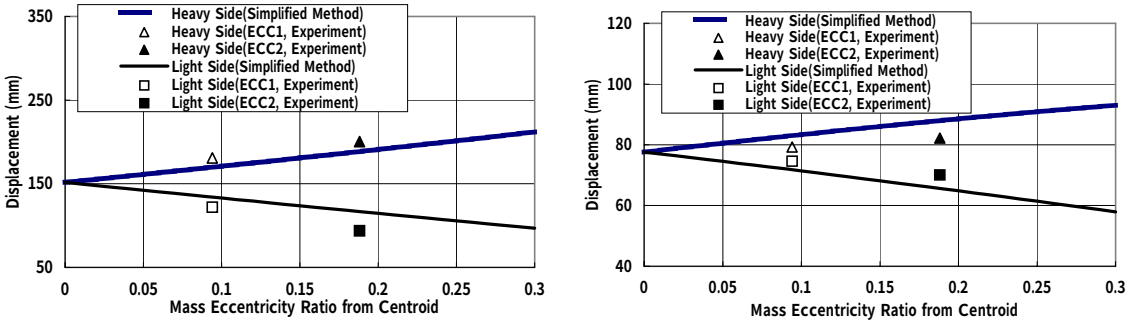

a) Rolling system b)Sliding system

Figure 9. Comparison of peak edge displacement responses

Similarly to Fig. 8, in Fig. 9 is shown the relationship between peak edge displacement response and the mass-eccentricity. As compared to the peak torsional angle, a much better agreement is observed here between the experimental results and those obtained by the analytical simulation for the rolling system. Most likely, this is related to the fact that peak torsional angle and peak edge displacements do not occur at the same instants.

5. CONCLUDING REMARKS

The effect of mass-eccentricity on the torsional response of base isolation systems for houses was investigated. Results indicate that torsional response of base isolated systems is not only a function of mass-eccentricity and earthquake ground motion characteristics, but is also very much dependent on the mechanical characteristics of the isolation systems. A remarkable difference between peak torsional angle responses of the rolling and sliding systems was observed. It appears that the sliding system is less sensitive to mass-eccentricity as compared to the rolling system.

ACKNOWLEDGEMENTS

The authors would like to express their sincere thanks to all the members of the committee on "Development of new technologies for seismic isolators for houses", the chairman of which is Mr. Shoichi Yamaguchi, president of Tokyo Kenchiku Structural Engineers, for providing data and valuable suggestions related to this study. The kind assistance of Dr. Keiichi Tamura, Public Works Research Institute in operating the shaking table is greatly appreciated.

REFERENCES

Iiba, M., Yamanouchi, H., Midorikawa, M., et al. (1998) "Research on Performance of Base Isolated House", *Proc. of the Second World Conference on Structural Control*, Kyoto, Japan, 2, pp1119-1126.

Iiba, M., Midorikawa, M., Kawai, M., et al. (1988) "Shaking Table Tests on Seismic Behavior of Isolators for Houses", *Proc. of the 10th Japan Earthquake Engineering Symposium*, Yokohama, Japan, pp2653-2658

Iiba, M., Midorikawa, M., Yamanouchi, H., et al. (2000) "Shaking Table Tests on Performance of Isolators for Houses Subjected to Three Dimensional Earthquake Motions", *Proc. of the 12 World Conference of Earthquake Engineering*, No.1765

Appendix 6

Section 6 *Sub-Structure Pseudo Dynamic Testing on 12 story Reinforced Concrete Frame with Soft First Story*

presented by H. Kuramoto

Sub-Structure Pseudo Dynamic Testing on 12 Story Reinforced Concrete Frame with Soft First Story

ICCEED, Toyohashi University of Technology

Hiroshi KURAMOTO

Motivation

The 1995 Kobe Earthquake damaged to many RC buildings with soft first story.

MOC revised some of the Notifications relating to RC buildings with SFS as action in an emergency.

More detailed examination is required to establish a rational evaluation method of seismic performance of the building.

Objectives

- To investigate causes of the collapse of the building and its mechanisms.
- To examine systems for preventing the collapse.
- To develop a rational evaluation method for the seismic performance of RC buildings with soft first story.

Method of Study

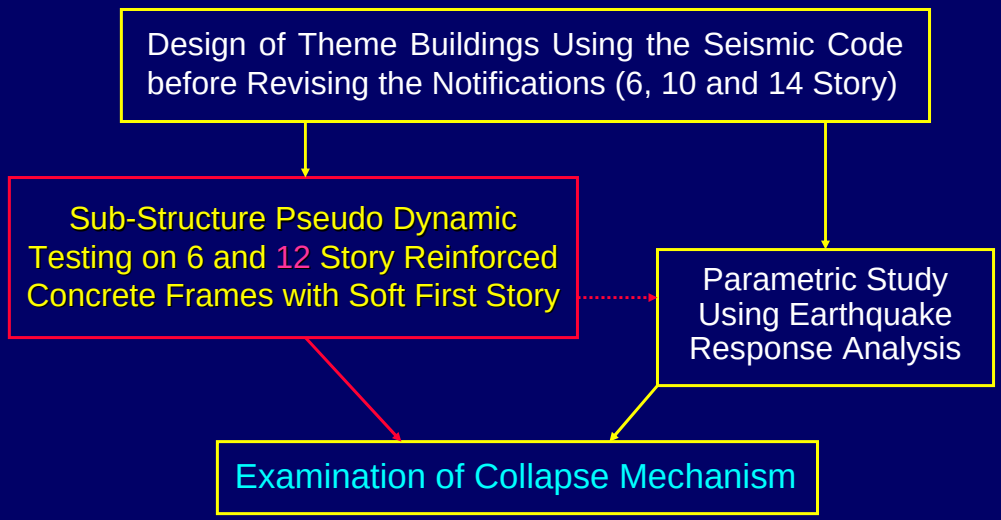

Prototype with the Scale of 1/2.5

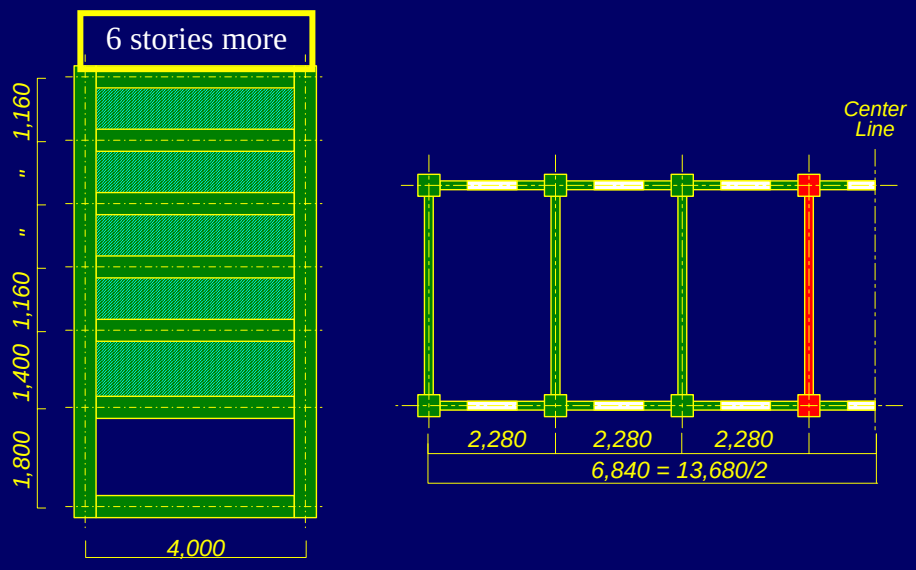

Test Specimen

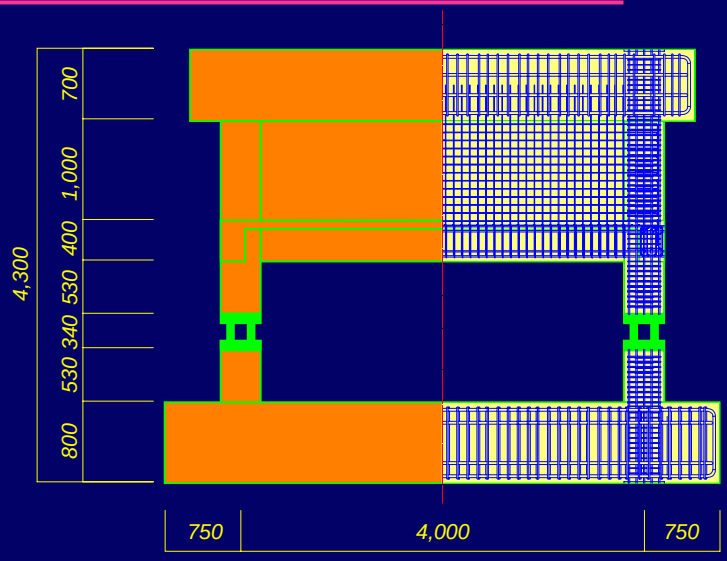

Load Cell to Measure the Shear and Axial Forces in Columns at the First Story

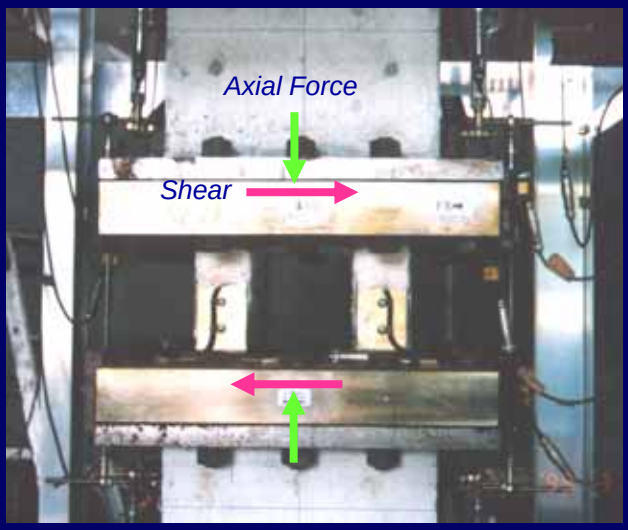

Loading Apparatus

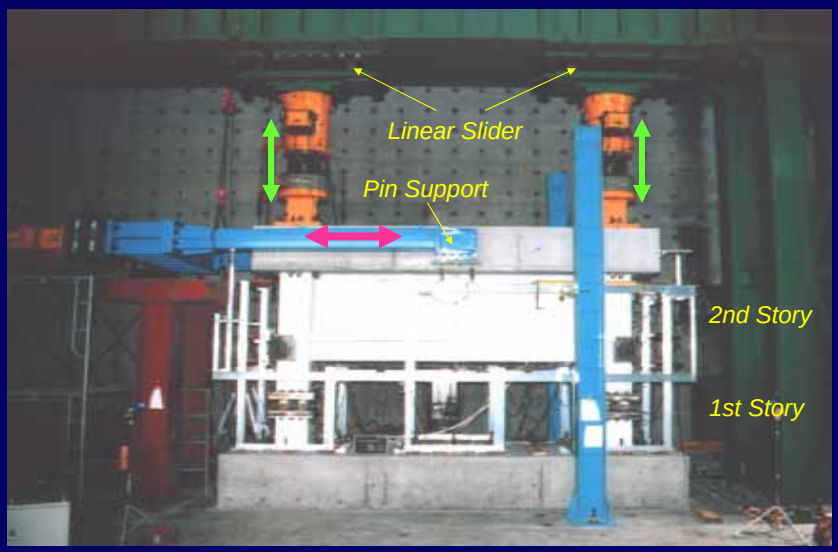

Input Ground Motions

- El Centro NS (1940) : 10 kine, 25 kine, 50 kine
- JMA-Kobe NS (1995) : original (90 kine)

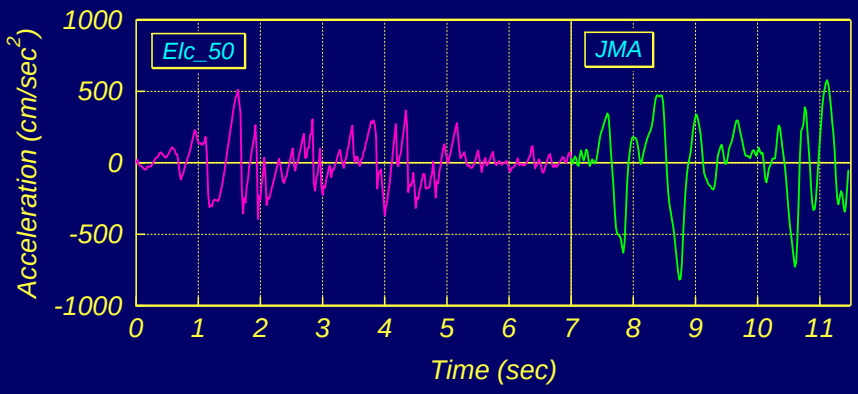

Failure of Columns at 1st Story

West Side

East Side

Failure of Columns at 1st Story

West Side

East Side

Failure of a Shear Wall at 2nd Story

West Side

East Side

Story Shear versus Story Drift Relation at the First Story

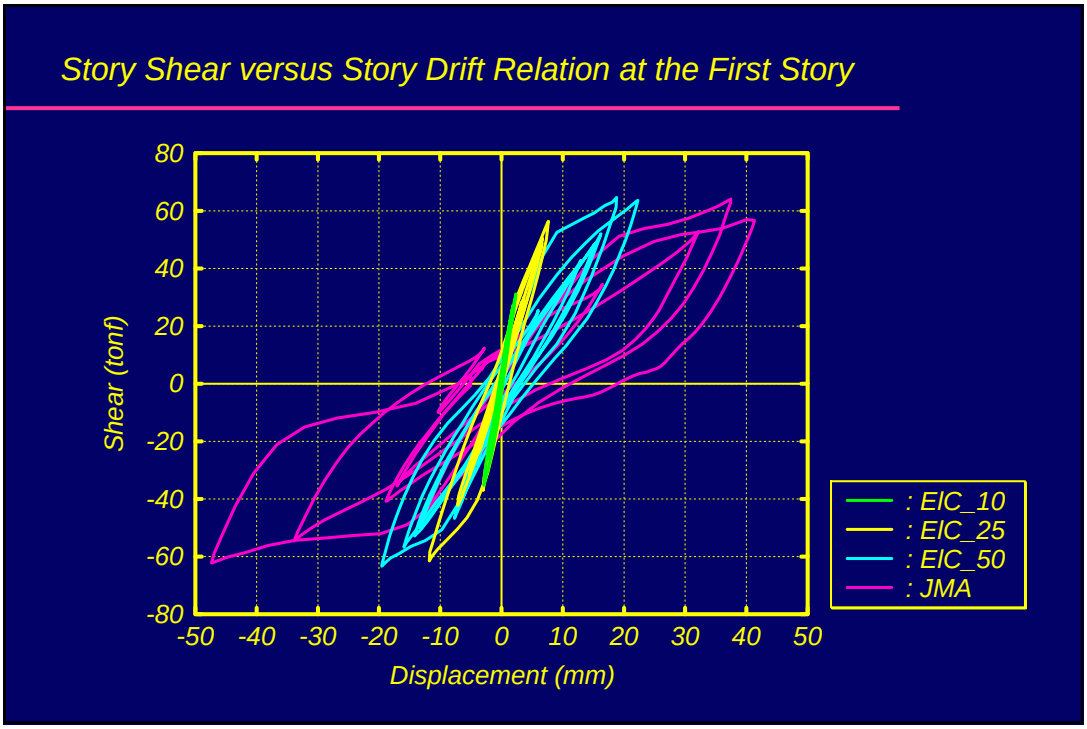

Axial Force – Shear – Story Drift Interaction of Columns

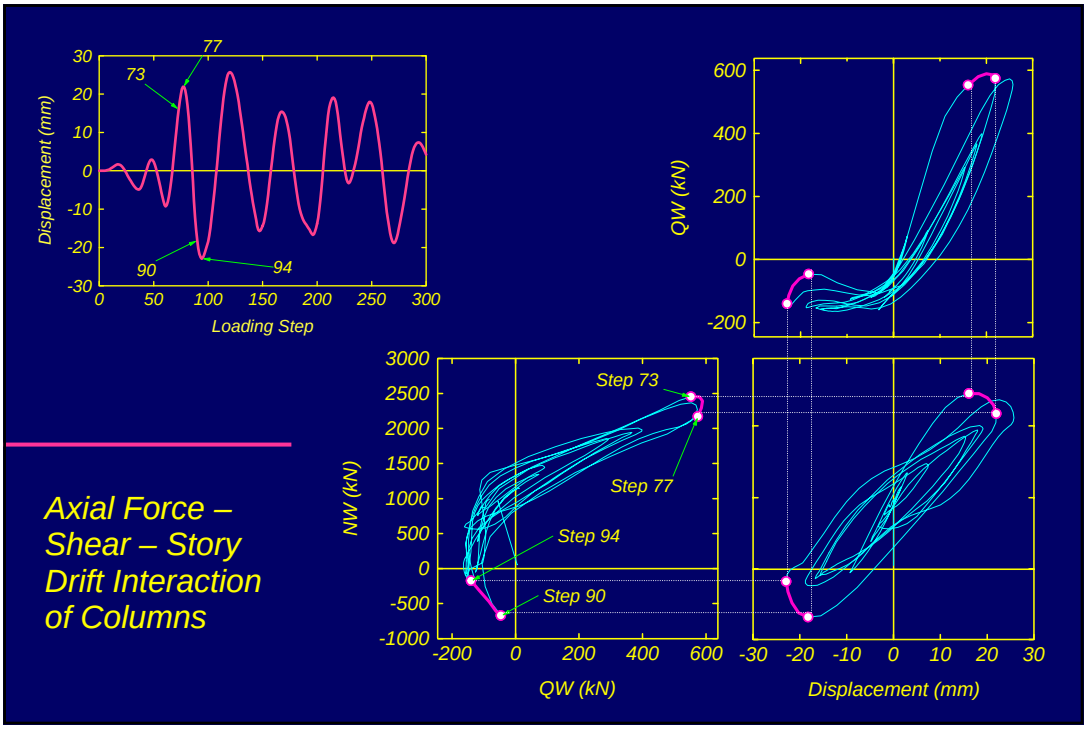

External Force Distribution and Displacement Distribution along Building Height

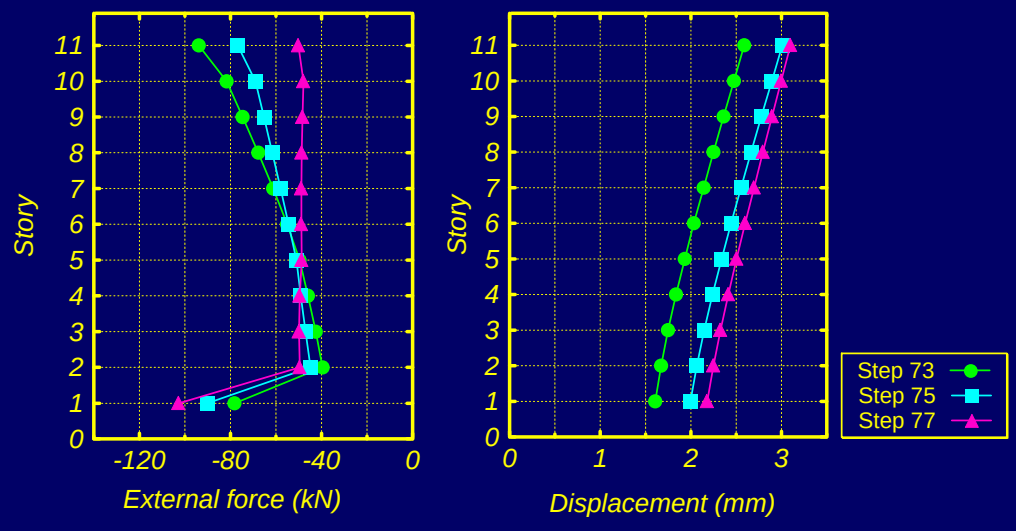

Conclusion

Sub-Structure Pseudo Dynamic Testing
on 12 Story Reinforced Concrete Frame with Soft First Story

- Collapse Mechanism：
  Story collapse mechanism in the 1st story with the flexural yielding of columns
- Maximum Story Drift Angle at the 1st story:
  1/63 for El Centro NS 50kine input and 1/29 for JMA-Kobe NS original input
- Axial Force Ratio of Columns at Maximum Response：-0.15～0.52
- External Force Distribution along the building height at Maximum Response：
  Uniform shape
- Higher mode effects are observed before reaching the maximum displacement response.